Nature of the stacking faults in orthorhombic $LiMnO_2$

Laurence Croguennec,[a] Philippe Deniard,[a] Raymond Brec[a] and André Lecerf[b]

[a]*Laboratoire de Chimie des Solides, I.M.N. UM 110 CNRS, 2 rue de la Houssinière, 44072 Nantes Cedex 03, France*
[b]*Laboratoire de Chimie des Solides, INSA, 20 avevue des Buttes de Couesnes, 35043 Rennes Cedex, France*

The synthesis of orthorhombic $LiMnO_2$ (O-$LiMnO_2$) with very small crystals (diameter ≈ 0.3 μm) leads to peculiar X-ray diffraction patterns. Some reflections (with k even) remain thin allowing for cell parameter refinements, showing that, compared to phases with bigger crystals, b and c remain unchanged, whereas an important increase of the a parameter is observed. Other reflections (with $k=2n+1$ and $h\neq 0$) are widened substantially, while the remnant peaks ($k=2n+1$ and $h=0$) undergo a strong asymmetrization. These features have been related successfully to faults corresponding to a $\boldsymbol{b}/2$ translation of a basic unit constituting O-$LiMnO_2$. A simulation made with the Diffax program allowed good reproduction of the experimental X-ray diffraction data, showing a statistic distribution of the faults, at least for the low fault concentrations corresponding to the samples under study. The insertion of the fault corresponds to the insertion of a monoclinic cell between two blocks of orthorhombic symmetry. This cell ($a\approx 5.53$ Å, $b\approx 2.80$ Å, $c\approx 5.30$ Å) corresponds to a newly obtained monoclinic $LiMnO_2$ phase obtained through a topotactic deintercalation of α-$NaMnO_2$. The fault percentage of the compounds studied goes from 1 to 6% and is well correlated to the substitution ratio between lithium and manganese when the fault occurrence is treated as a cationic disorder (only in the case of small disorder for which the lines remain treatable with the Rietveld refinement program). The fault percentage can also be determined easily from the cell parameter relation $a=x_0a_0+x_ma_m\sin\gamma$, where a_0 and a_m are the parameters of the orthorhombic and monoclinic cell of the pure phases and x_0 and x_m their relative fractions, a being the parameter of the faulted phase as refined from the fault-unaffected thin reflection peaks.

Since the higher electrochemical capacities of orthorhombic $LiMnO_2$ (O-$LiMnO_2$) used in lithium batteries have been related to small crystal size,[1] attempts have been made to decrease the O-$LiMnO_2$ crystal size as much as possible in order to obtain cathodic materials with still higher capacities. Under certain experimental conditions, the synthesis of O-$LiMnO_2$ may lead to preparations containing some $LiMn_2O_4$ spinel impurity.[2] Based on the usual X-ray diffraction analyses, these spinel-containing O-$LiMnO_2$ compounds show XRD patterns similar to those obtained for the pure samples, except that their X-ray diffraction lines appear generally very ill defined. This was first ascribed to a poor crystallization state due to very small crystals with short coherence lengths, which was related to the synthesis procedures. These materials showed particularly good electrochemical behaviour, and questions arose about the respective roles of the crystal size *vs.* the spinel content.

Going beyond the simple observation of the widening and distortion of the diffraction peaks, this study led us to determine the true origin of the structural phenomenon responsible for the X-ray pattern characteristics. This article thus describes the nature and the extent of the faults found in O-$LiMnO_2$ samples (with and without spinel impurity) and demonstrates how these faults can satisfactorily model the XRD pattern features of the phases for various fault concentrations. It is also demonstrated that the spinel presence seems only to be an indicator (but an important one) of the particle size.

Experimental

A series of six samples (labelled as shown in Table 1) containing mostly the spinel $LiMn_2O_4$ as impurity have been synthesized under conditions very similar to those used to prepare X-ray diffraction pure O-$LiMnO_2$.[1] The usual synthesis time was shortened in order to try to decrease the crystallinity of the phases. The samples were prepared from mixtures of Mn_2O_3 [obtained by pyrolysing MnO_2 (Sedema T.R.)] and $LiOH\cdot H_2O$ (Chemetals) with Li/Mn ratios varying from 0.83 to 0.99. The ground powders of the starting phases were placed in an aluminium boat in a nitrogen-filled silica tube. Some oxygen was added to obtain the targeted mean manganese oxidation states. The samples were heated at 500 °C for 5 h, ground after cooling and heated again at 700 °C for 10 h, before final slow cooling (10 h) to room temperature. Under these conditions, samples with different $LiMn_2O_4$ contents were obtained (Table 1).

Mn and Li elemental analyses were carried out by EDTA complexation and emission plasma spectrometry, respectively, whereas the mean oxidation states of manganese were determined by oxidoreduction analysis using Fe^{2+} as the reducing agent. It was found that increasing lithium content corresponded to the decreasing manganese oxidation state, in agreement with a decreasing spinel content (Table 1).

The X-ray diffraction patterns were recorded on a Siemens D5000 diffractometer, without monochromator (Cu-Kα_1 = 1.540598 and Cu-Kα_2 = 1.544390 Å) in Bragg–Brentano geometry.

The X-ray patterns showed that the sample mixtures were mostly made up of O-$LiMnO_2$ with some $LiMn_2O_4$ spinel. A small amount of tetragonal $Li_2Mn_2O_4$ and Mn_3O_4 could also be detected. A Rietveld quantitative analysis[3,4] was carried out to determine the percentage of each phase present (see later).

The Diffax program[5] allows the calculation of the diffracted intensities of crystals containing imperfections such as twinning and/or two-dimensional stacking faults. This software was chosen to model the poorly defined X-ray diffraction pattern of O-$LiMnO_2$. Diffax is a modelling, not a refinement, program; it is necessary to make hypotheses and to compare visually the calculated and observed X-ray powder diffraction diagrams. To calculate the structure factors, it is thus necessary to know not only the imagined layers sequences, but also the transition probability α_{ij} between two layers i and j within the stacks, and the interlayer translational vectors R_{ij}. The structural data of O-$LiMnO_2$ (cell parameters, atomic positions and pseudo-Voigt u,v,w and η profile function parameters) were determined from the Rietveld refinement performed with the Fullprof program.

Table 1 Manganese and lithium elemental analyses of several samples (O-$LiMnO_2$–$LiMn_2O_4$ mixtures) with nominal and experimental Li/Mn ratios

	MN438	MN436	MN440	MN435	MN439	MN441
$(Li/Mn)_{nom.}$	0.83	0.91	0.93	0.94	0.98	0.99
Li (%)	6.01	6.66	6.85	6.97	7.24	7.14
Mn (%)	58.70	58.43	58.24	58.74	58.30	57.55
$(Li/Mn)_{exp.}$	0.81	0.90	0.93	0.94	0.98	0.98
Mn mean oxidation state[a]	3.18	3.08	3.07	3.05	3.03	3.01
D_{200}[b]/Å	185	205	205	210	185	235
D_{002}[b]/Å	270	235	210	230	235	240

[a]The mean manganese oxidation state are results from redox analyses. [b]Coherence lengths (D) calculated using the Warren–Averbach method (ref. 6).

Characterization of O-$LiMnO_2$ samples

The sample colour changed from light to dark green with increasing spinel content. In our studies, in contrast to what had been observed before,[1] the colour change is not due to the crystallite size but rather to the $LiMnO_2/LiMn_2O_4$ ratio. In effect, the crystallite and crystal size of the six samples as calculated by the Warren–Averbach method[6] on those peaks not affected by the stacking faults in the compounds (see below) and observed by scanning electron microscopy (diameter ≈ 0.3 μm) (Fig. 1) were found to be about the same. The crystallite size was *ca.* 200 Å in the a and c directions (Table 1).

The XRD patterns of these newly prepared spinel-containing orthorhombic O-$LiMnO_2$ phases (Fig. 2) showed important changes compared to those of the well crystallized spinel-free samples studied previously.[1] In effect, one observes a marked widening of certain peaks, leading to the disappearance of the weaker lines (see, for example, lines around $2\theta \approx 23°$ and 41°), and a strong asymmetry of others towards high θ values. Using the orthorhombic cell parameters of a well crystallized and characterized O-$LiMnO_2$ phase, an attempt to index and model the profiles of all the diffraction lines failed: only the narrow and symmetric peaks could be considered, the widening and asymmetry of the other peaks preventing any fit. Narrow peaks correspond to the planes with k even, and their profile modelling with a pseudo-Voigt-type function with the help of the PROLIX[7] program was carried out successfully (see Table 2 given as an example for the sample MN438). Enough of these peaks were left out to allow the cell parameter refinement of the six samples under study (program U-FIT[8]) (Table 3). Whereas the b and c parameters are identical to those of pure O-$LiMnO_2$, an important increase of *ca.* 0.3% of the a parameter is recorded for these spinel impurity containing samples. The widened reflections not taken into account in the refinement procedure correspond to $k = 2n+1$ and $h \neq 0$ and the asymmetric ones to $k = 2n+1$ and $h = 0$ (Fig. 2). In the case of the asymmetric lines, even a Thomson–Cox–Hasting[4] type of modelling did not work because of the very strong right-side asymmetry of the diffraction lines.

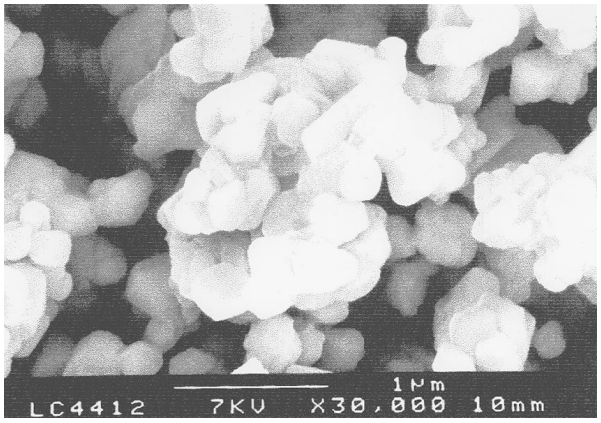

Fig. 1 Electronic microscope photographs of one spinel containing O-$LiMnO_2$ sample (ref. MN441) showing the regular size distribution (diameter ≈ 0.3 μm) of the crystals

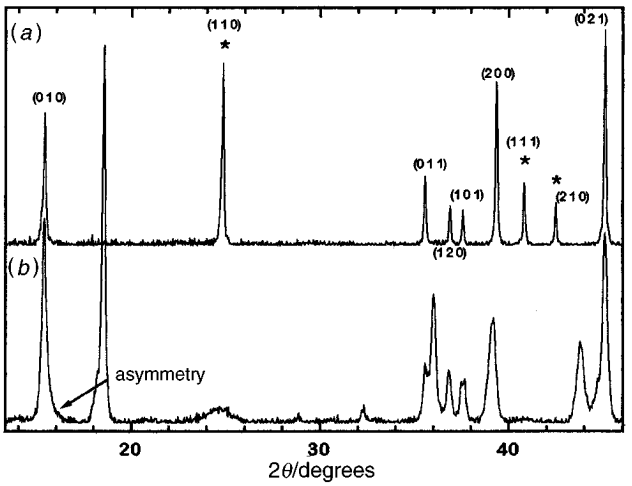

Fig. 2 Comparison between the X-ray diffraction pattern of (*a*) a 'pure' O-$LiMnO_2$ (ref. MN412)[1] and (*b*) the spinel-containing MN438 sample. Widening and asymmetry of certain peaks are clearly observed. The extra reflections on the diagram of the latter sample are due to the occurrence of $LiMn_2O_4$, $Li_2Mn_2O_4$ and Mn_3O_4. Peaks marked with asterisks are enlarged strongly.

Table 2 Profiles fitting obtained from the MN438 sample X-ray diffraction pattern with the PROLIX program (only the reflection lines of O-$LiMnO_2$ are given)[a]

hkl	2θ/degrees	*d*/Å	*I*	FWHM/degrees	η
010	*15.37(3)*	*5.76(1)*	*100.00*	*0.2721*	*0.857*
110	*25.0(3)*	*3.57(5)*	*38.30*	*1.5720*	*0.045*
011	*35.57(7)*	*2.522(5)*	*20.23*	*0.2687*	*0.000*
120	36.84(6)	2.438(4)	29.85	0.2860	0.982
101	37.58(8)	2.391(5)	22.60	0.3672	0.000
200	39.13(3)	2.300(2)	69.15	0.4432	0.071
111	—	—	—	—	—
210	—	—	—	—	—
021	45.10(2)	2.0089(8)	97.75	0.3026	0.665
211	—	—	—	—	—
221	61.26(3)	1.5119(8)	55.54	0.3915	0.319
131	—	—	—	—	—
040	64.8(2)	1.439(3)	12.32	0.4644	0.000
002	66.6(2)	1.404(3)	7.57	0.2806	0.360
112	—	—	—	—	—
240	78.47(6)	1.2178(8)	9.43	0.3727	0.000
202	80.11(5)	1.1970(6)	8.46	0.2900	0.000

[a]Entries in italics correspond to those peaks which were too wide and too asymmetric to be considered in the parameter refinements. Non-fitted lines are those which were so broad that they were lost in the background.

These different features of the 'non-classical' reflection peaks (shift, widening, asymmetry) are well documented in the case of the γ-MnO_2 series[9,10] and have been explained through stacking faults resulting from the alternating of pyrolusite and

Table 3 Least-squares refinement of the O-$LiMnO_2$ cell parameters for the six samples under study; comparison with the parameters refined for a well crystallized pure O-$LiMnO_2$ sample (from ref. 1)

	MN438	MN436	MN440	MN435	MN439	MN441	Hoppe	ref. 1
a/Å	4.593(2)	4.593(1)	4.593(1)	4.5904(7)	4.604(3)	4.5903(9)	4.572	4.5792
b/Å	5.754(2)	5.747(1)	5.750(1)	5.7462(9)	5.759(5)	5.754(2)	5.757	5.7509
c/Å	2.8061(9)	2.8051(5)	2.8045(5)	2.8044(3)	2.8088(9)	2.8067(6)	2.805	2.8060
V/Å^3	74.15(8)	74.05(5)	74.07(5)	73.97(3)	74.5(1)	74.13(5)	73.8	73.89

ramsdellite blocks. Accordingly, De Wolff[9] described the γ-MnO_2 phases as a statistic distribution of simple and double chains. Following the same idea, we studied the possible occurrence of stacking faults in the O-$LiMnO_2$ materials.

Quantitative analysis of sample mixtures

The phases present in the samples under study contained essentially the O-$LiMnO_2$ majority phase and the spinel $LiMn_2O_4$ minority one. Some small amounts of tetragonal $Li_2Mn_2O_4$ and Mn_3O_4 could also be detected. The percentage of each phase was calculated, whenever possible, by using the Fullprof program. Rietveld analyses were carried out with some specific constraints because of the particularities of the diagram line shapes as explained above. The refinement conditions were as follows: angular regions were excluded from the refinement for those peaks widened, markedly; the atomic positions, cell parameters and profile function parameters were refined only in the case of O-$LiMnO_2$ and $LiMn_2O_4$; owing to the very small amounts of Mn_3O_4 and $Li_2Mn_2O_4$, only the cell parameters were refined in these cases. For these two compounds, the profile function parameters were not allowed to vary with θ. The atomic parameters were in agreement with those of the literature.[11,12]

Obviously, and owing to the complexity of the sample compositions, the quality of the refinement proved not perfect, but it seemed to us to be of sufficient quality to quantify the ratio of the four phases. A validation of the multiple excluded regions procedure was performed by refining the structure of pure O-$LiMnO_2$. It was found that the exclusion of domains of the same magnitude as those considered for the mixed-phase samples resulted essentially in the lowering of the data accuracy, without sizeable drift of the atomic positions.

The quantitative analyses were easy to carry out owing to the similar compositions of the phases and their similar linear absorption coefficients (in which case the Brindley coefficient[13–15] can be considered equal to unity).

Table 4 gives the quantitative analyses of the six samples. It can be seen that the mean oxidation states of manganese calculated from the phase percentages agree well with those determined by the redox analyses. Note also that only one phase out of the six exhibited a measurable amount of Mn_3O_4 [5.3(6)%].

Determination of stacking faults in O-$LiMnO_2$

O-$LiMnO_2$ structure and fault choice

Fig. 3 shows the O-$LiMnO_2$ structure projected along the b axis (with $a \approx 4.58$ Å, $b \approx 5.75$ Å, $c \approx 2.80$ Å). One can consider

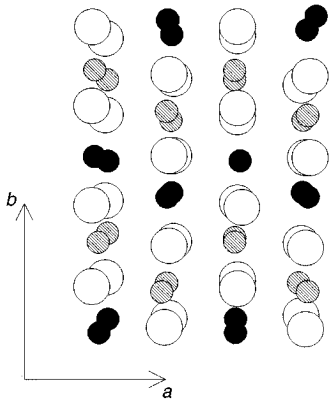

Fig. 3 Projection along the c axis of the structure of O-$LiMnO_2$. The phase can be described as a stacking, along b, of corrugated layers of oxygen, lithium, oxygen and manganese.

the structure as based on the stacking of very similar layers made of O/Li/O/Mn/O rows perpendicular to the Fig. 3 plane projection, the layers being stacked along the a axis. In order to describe the faults in O-$LiMnO_2$, four different basic units with the parameters $a/2$, b and c with the atomic arrangements shown in Fig. 4 have been chosen. Table 5 shows the atomic positions for the four units. Units 1, 3 and 2, 4 are structurally identical but are defined by their distinct transition probability

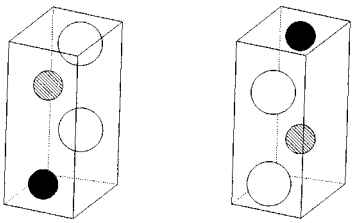

Fig. 4 Perspective views of the layers chosen to describe the faulted O-$LiMnO_2$

Table 5 Atomic coordinates of the four layers of the stacking faults

	layer 1 (≡3)	layer 2 (≡4)
Mn	1/2,*ca.*0.63,1/4	1/2,*ca.*0.37,3/4
Li	1/2,*ca.*0.10,1/4	1/2,*ca.*0.90,3/4
O(1)	1/2,*ca.*0.87,3/4	1/2,*ca.*0.13,1/4
O(2)	1/2,*ca.*0.39,3/4	1/2,*ca.*0.61,1/4

Table 4 Ratios of O-$LiMnO_2$, $LiMn_2O_4$, $Li_2Mn_2O_4$ and Mn_3O_4 in the different samples under study, with the calculated and measured manganese mean oxidation states

	MN438	MN436	MN440	MN435	MN439	MN441
$LiMnO_2$ (%)	67(3)	86(3)	90(2)	92(3)	96(3)	99(2)
$LiMn_2O_4$ (%)	22(1)	10.3(7)	8.1(5)	5.6(5)	2.3(3)	0.9(2)
$Li_2Mn_2O_4$ (%)	5.7(7)	3.4(7)	2.2(5)	2.1(5)	2.0(4)	—
Mn_3O_4 (%)	5.3(6)	—	—	—	—	—
Mn calc. mean oxidation state	3.12	3.09	3.07	3.05	3.02	3.01
Mn exptl. mean oxidation state	3.18	3.08	3.05	3.05	3.03	3.01

α_{ij} and their translation vector R_{ij}. The occupation ratios of all positions were equal to unity and the atomic displacement parameters were 0.5 Å^2 for Mn and 1.0 Å^2 for Li and O.

Because of the O-$LiMnO_2$ atomic arrangement, we first tested the possibility of a fault resulting from a translation of $\boldsymbol{b}/2$ of a basic unit. The transition probability α_{ij} between two layers i and j and the translation vectors R_{ij} are given in Table 6.

Results of simulation

Fig. 5(*a*) shows the simulated X-ray diffraction pattern obtained from the proposed fault (translation of a slab of $\boldsymbol{b}/2$), the fault concentration going from 0 to 1. Fig. 5(*b*) shows the strong influence of even small amounts of faults. Also, the main characteristics of the ill defined diagrams obtained for the six samples under study are very well reproduced, with in particular a marked asymmetry on the right of certain peaks [*e.g.* (010)] and very strong widening of others [*e.g.* (110), (111) and (210)]. Clearly, one of the first main lines of the diagrams, the (110) peak, is highly sensitive to even small stacking faults. This rules out the first explanation given for this peak broadening through the occurrence of some Mn_2O_3 impurity.[1] This model is thus to be considered to account for the structural arrangement of faulted O-$LiMnO_2$. Indeed, other types of faults were considered but proved to be unable to show the expected influence on the X-ray diffraction pattern.

Consequences of the occurrence of faults in O-$LiMnO_2$

The insertion of the fault corresponds to the occurrence of a monoclinic cell between two blocks of orthorhombic symmetry. The so-called 'fault cell' has, then, an a_m parameter defined as: $\boldsymbol{a}_m = \boldsymbol{a}_0 - \boldsymbol{b}_0/2$ (Fig. 6), while b_0 and c_0 still correspond to the translation of the well ordered phase network. Indeed, this interpretation holds only for small amount of faults, *i.e.* in the case of isolated faults, which is the case here [Fig. 5(*a*)]. This model implies that the diffraction patterns observed yield the mean structure, the a parameter observed corresponding to the weighted average of the parameters a_0 and $a_m \sin\gamma$ of the orthorhombic and monoclinic cells. Fig. 7 shows the orthorhombic and monoclinic $LiMnO_2$ reciprocal networks projected along the $\boldsymbol{c}$ axis, an identical vector for both symmetries. For even k, the diffraction lines will be neither shifted nor widened since both lattice nodes fall at the same positions [peaks (120), (101) and (200), for instance]. Clearly, and as can be shown through simulation with a random distribution of faults, the concentration of which can be simulated up to

Table 6 Values attributed to the transition probability α_{ij} and translation vector R_{ij} between two layers i and j allowing the description of the chosen fault [the x values (between 0 and 1) allow for the probability variation of the faults]

transition	α_{ij}	R_{ij}
1–1	0.000	—
1–2	$1-x$	$a/2$
1–3	0.000	—
1–4	x	$a/2+b/2$
2–1	0.000	—
2–2	0.000	—
2–3	1.000	$a/2$
2–4	0.000	—
3–1	0.000	—
3–2	$1-x$	$a/2$
3–3	0.000	—
3–4	x	$a/2+b/2$
4–1	1.000	$a/2$
4–2	0.000	—
4–3	0.000	—
4–4	0.000	—

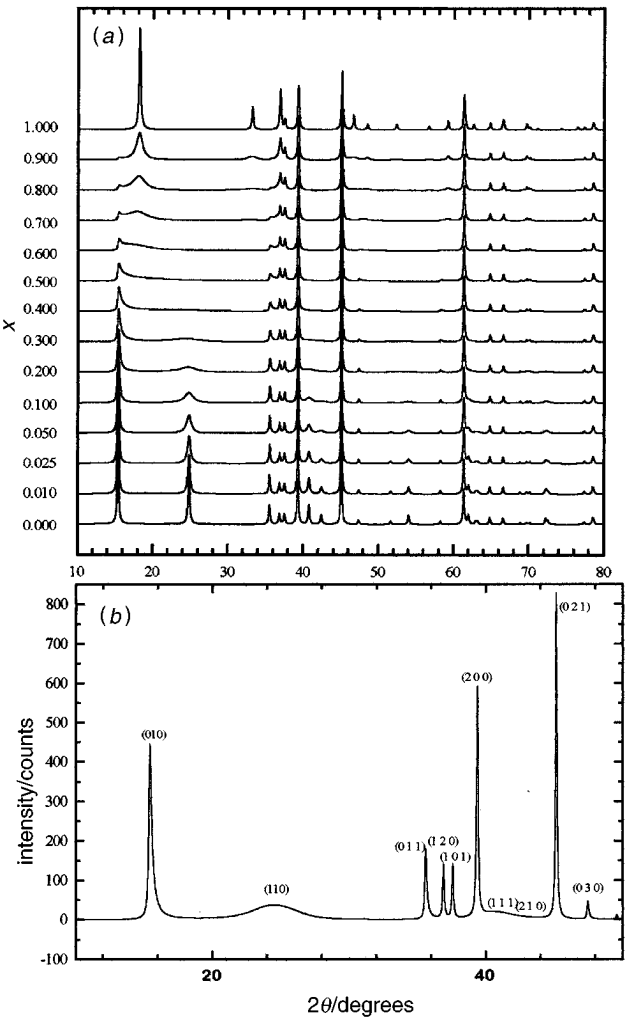

Fig. 5 (*a*) Simulated X-ray diffraction patterns for O-$LiMnO_2$ with faults corresponding to a $\boldsymbol{b}/2$ translation of an isolated slab (lowermost pattern, orthorhombic $LiMnO_2$; uppermost pattern, monoclinic $LiMnO_2$). The simulation was made for fault contents from 0 to 1. (*b*) For a 0.1 fault concentration, one can see the marked asymmetry of the (010) and (030) peaks and the important widening of the (110), (111) and (210) lines.

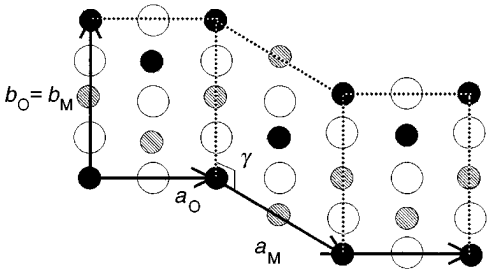

Fig. 6 Projection along the c axis of the orthorhombic cell of O-$LiMnO_2$ with the inserted monoclinic fault

100% (*i.e.* up to pure monoclinic $LiMnO_2$) [Fig. 5(*a*)], those lines not affected by the faults are reflections common to the two phases. For odd k and $h \neq 0$, the nodes of the monoclinic cell are in between two nodes of the orthorhombic cell. For the reflections (h, $k=2n+1$, l) there results a widening corresponding to the shorter and longer diffusion vectors on each side of the orthorhombic cell vector. This is what is observed for the lines (110), (111) and (210), for instance. For odd k and $h=0$, the nodes of the monoclinic cell are also in between two nodes of the orthorhombic cell, but the diffusion vector is longer on each side of the orthorhombic cell vector. This results in an increase of the diffusion vector which induces a

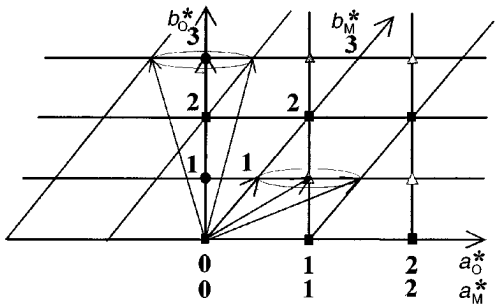

Fig. 7 Projection along the *c* axis of the reciprocal networks of O-$LiMnO_2$ and of the fault cell M-$LiMnO_2$. The circles correspond to the peaks presenting a strong right-side asymmetry, the squares correspond to the peaks keeping their normal profile (nodes common to both networks), and the triangles represent the peaks enlarged strongly.

marked asymmetry towards the higher diffraction angles, *i.e.* on the right side of the (0, $k=2n+1$, l) peaks (see Fig. 7).

Fig. 8 shows the calculated pattern of a faulted O-$LiMnO_2$ phase (2.5% faults) compared with the experimental one. This simulation demonstrates how well reproduced the experimental data are (see how the fine but also abnormal lines are well modelled), allowing for a good evaluation of the faults concentration in a given sample. This evaluation is carried out by simple visual comparisons between several simulated diagrams and the diagram under study [see also below the (110) linewidth *vs.* the fault content].

Fig. 9 represents the projection along *c* of the $LiMnO_2$ monoclinic fault structure. This new structure represents an anionic ABC close stacking with a succession of lithium and manganese layers, these two cations remaining in octahedral sites. This structural arrangement is that of α-$NaMnO_2$[16] and this is confirmed by recent works[17,18] reporting the successful synthesis of isotypic monoclinic $LiMnO_2$ (M-$LiMnO_2$) by a topotactic substitution of sodium by lithium. In M-$LiMnO_2$, Li and Mn are in the (2d) positions of the $C2/m$ space group (0,1/2,1/2 and 0,0,0, respectively, for the atomic coordinates), whereas the oxygen atoms are in (4i) with $x\approx0.25$ and $y\approx0.75$ [these values are precisely calculated at 0.270(1) and 0.772(1) from the structure calculation of ref. 17]. Table 7 compares the estimated M-$LiMnO_2$ parameters of this study with those of the Rietveld refinement.

Scaling of stacking faults in O-$LiMnO_2$

The fault percentage can easily be determined from the relation $a=x_0a_0+x_ma_m\sin\gamma$, where a_0 and a_m are the parameters of the orthorhombic and monoclinic cells and x_0 and x_m their respective fractions. The knowledge of a and of a_0 (taken as 4.572 Å from a single-crystal study)[19] allows the determination of all the fault concentrations of the samples under study along with the spinel-free samples studied in a previous work[1] (Table 8). It appears that the phases containing $LiMn_2O_4$ in detectable amounts (0.9–22%) exhibit a large number of faults from 3.4 to 6.1%, whereas the spinel-free materials[1] (at least at the X-ray diffraction detection threshold level, but simulations show that this threshold can be as low as 0.4%) contain percentages lower than 2.9%, with a sample at 0.9%. If the presence of $LiMn_2O_4$ is indicative of a more disordered O-$LiMnO_2$, (probably due to a particular synthesis process), it is also of interest to observe that the spinel concentration is not well correlated to that of the faults, although it can be seen that the less faulted compounds contain no spinel.

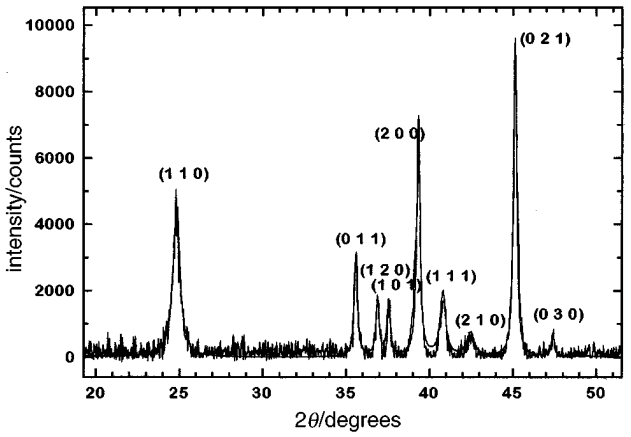

Fig. 8 An example of the very good agreement between the simulated and experimental X-ray diffraction patterns for 2.5% faults in O-$LiMnO_2$ (sample MN384 from ref. 1)

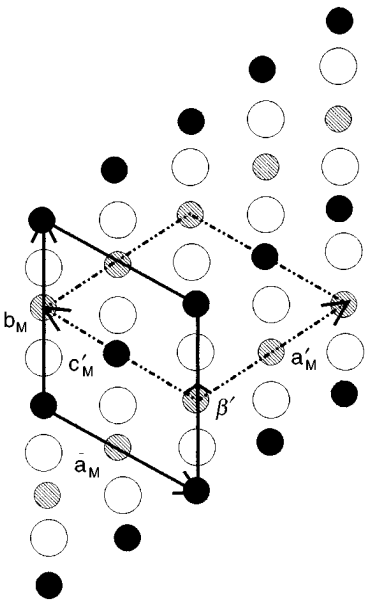

Fig. 9 Projection along the *c* axis of monoclinic $LiMnO_2$ corresponding to the fault found in O-$LiMnO_2$. The parameters of the broken lines cell allow a description in the monoclinic M-$NaMnO_2$-type reference axes.

Table 7 Comparisons between the monoclinic cells of α-$NaMnO_2$, the $LiMnO_2$ fault in O-$LiMnO_2$, and M-$LiMnO_2$ prepared *via* a soft chemistry route

	α-$NaMnO_2$	$LiMnO_2$(fault)[a]	M-$LiMnO_2$[b]
a/Å	5.63(1)	*ca.*5.53	5.439(3)
b/Å	2.86(4)	*ca.*2.80	2.809(2)
c/Å	5.77(1)	*ca.*5.30	5.395(4)
β/degrees	112.9(5)	116	115.9(4)

[a]Only approximate values can be given for the fault cell, since it is only a model used in Diffax. [b]Ref. 17.

Table 8 Estimated fault concentrations of the monoclinic $LiMnO_2$ type in orthorhombic $LiMnO_2$ for the six samples under study

spinel-free samples[a]		this study		
sample	faults(%)	sample	$LiMn_2O_4$(%)	faults(%)
MN389	1.7	MN441	0.9	3.4
MN384	2.5	MN439	2.3	6.0
MN386	2.9	MN435	5.6	5.4
MN399	1.1	MN440	8	4.8
MN401	1.4	MN436	10	6.2
MN412	0.9	MN438	22	6.1

[a]Ref. 1.

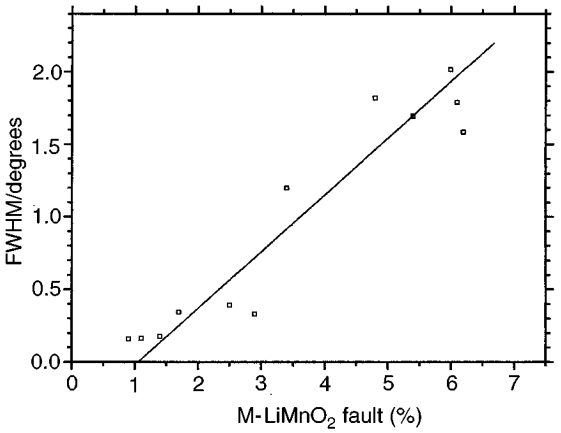

Fig. 10 Evolution of the (110) peak full width at half maximum as a function of the fault percentage. All the samples of this study have been considered along with spinel-free samples from a previous study.[1]

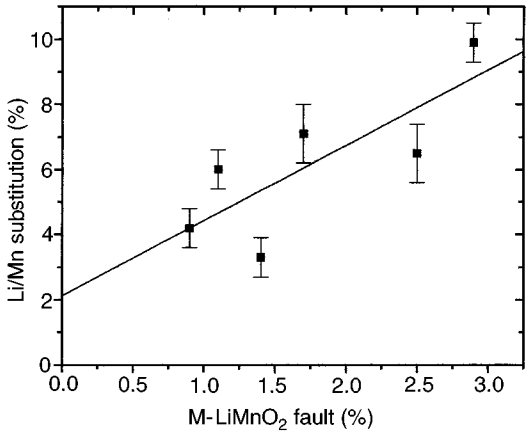

Fig. 11 Variation of the Li/Mn substitution ratio *vs.* the fault percentage in pure O-$LiMnO_2$ obtained previously.[1] Within the estimated standard deviation, the zero fault compound corresponds to zero substitution ratio.

Since some X-ray reflections of O-$LiMnO_2$ are very sensitive to monoclinic fault occurrence, it was of interest to see whether one could quantify easily the fault concentration without modelling the diagrams. Fig. 10 shows the variation of the more disorder-sensitive (110) linewidth *vs.* the fault content. A clear correlation exists and one can see that the (110) linewidth at half maximum is a good measure of the fault occurrence.

The presence of the stacking faults found in O-$LiMnO_2$ is in perfect agreement with the previous cationic disordered model chosen to better refine the diffraction data:[1] the slab shift is approximately equivalent to a cationic substitution (see Fig. 3). To prove the point further, Fig. 11 shows the good correlation between the Li/Mn 'substitution' ratio and the fault concentration. It should be recalled (see ref. 1) that in a previous study and for slightly faulted materials, the diagrams had been refined by the Rietveld program, the faults showing up as Li/Mn disorder. For a hypothetical zero-fault material, the substitution ratio is, within error, equal to zero, as expected. The Li/Mn substitution had been considered as a completely random distribution. The present structural study demonstrates that the disorder is in fact based on a well identified shear mechanism, involving entire slabs shifts.

The recently synthesized M-$LiMnO_2$ phase[17] also shows a Li/Mn substitution ratio of *ca.* 3%: it is thus possible that this disorder originates in the occurrence of orthorhombic faults. This situation would then be similar to that of O-$LiMnO_2$, and one may wonder whether a continuous increase of faults would allow an intergrowth phase for a high fault ratio (25, 50, 75%, for instance). Beyond these structural considerations, the influence of these faults on the electrochemical behaviour of O-$LiMnO_2$ as a cathodic material in lithium batteries is under study and will be the subject of a forthcoming article.

Conclusions

Two previous groups[2,20] had proposed the hypothesis of stacking faults occurring in O-$LiMnO_2$. We have obtained evidence for their existence and have identified their nature. In agreement with their random distribution, these faults model very well the experimental X-ray diffraction patterns and explain the widening and asymmetrization of certain reflection lines. This study emphasizes the rather systematic behaviour of the manganese oxides to exhibit structural disorders in their structures. These disorders are very sensitive to the synthetic procedures which must be tightly controlled to obtain the targeted materials. In particular, smaller crystals correspond to higher fault concentrations, with the occurrence of spinel impurity. Since the stacking faults and the crystal size are expected to influence greatly the electrochemical behaviour of the manganese oxides, it is now important to relate the sample structural features to the electrochemical characteristics of faulted O-$LiMnO_2$.

The authors thank F. Boucher for helpful discussion and J. Gareh for his help in handling the Diffax program.

References

1 L. Croguennec, P. Deniard, R. Brec and A. Lecerf, *J. Mater. Chem.*, 1995, **5**, 1919.
2 J. N. Reimers, E. W. Fuller, E. Rosen and J. R. Dahn, *J. Electrochem. Soc.*, 1993, **140**, 3396.
3 H. M. Rietveld, *J. Appl. Crystallogr.*, 1969, **2**, 65.
4 J. Rodriguez-Carjaval, Fullprof Manual, ILL Report, 1992.
5 M. M. Treacy, M. W. Deem and J. M. Newsam, Diffax, V1.76, 1990.
6 B. E. Warren, in *Progress in Metal Physics*, Pergamon Press, London, 1959, vol. 8, p. 521.
7 M. Evain, J. M. Barbet, P. Deniard and R. Brec, presented at the *Powder Diffraction Meeting*, Toulouse, France, 1990.
8 M. Evain, U-FIT Manual, I.M.N. Internal Report, Nantes, France, 1992.
9 P. M. De Wolff, *Acta Crystallogr.*, 1959, **12**, 341.
10 M. Ripert, Thesis, I.N.P.G., Grenoble, 1990.
11 D. Jarosch, *Mineral. Petrol.*, 1987, **37**, 15.
12 W. I. F. David, M. M. Thackeray, L. A. De Picciotto and J. B. Goodenough, *J. Solid State Chem.*, 1987, **67**, 316.
13 R. J. Hill and C. J. Howard, *J. Appl. Crystallogr.*, 1987, **20**, 467.
14 D. L. Bish and S. A. Howard, *J. Appl. Crystallogr.*, 1988, **21**, 86.
15 G. W. Brindley, *Philos. Mag.*, 1945, **36**, 347.
16 J. P. Parant, R. Olazwaga, M. Devalette, C. Fouassier and P. Hagenmuller, *J. Solid State Chem.*, 1971, **3**, 1.
17 C. Delmas, personal communication.
18 A. R. Amstrong and P. G. Bruce, *Nature* (*London*), 1996, **381**, 499.
19 R. Hoppe, G. Brachtel and M. Jansen, *Z. Anorg. Allg. Chem.*, 1975, **417**, 1.
20 T. Ohzuku, A. Ueda and T. Hirai, *Chem. Express*, 1992, **7**, 193.

Paper 6/04947H; *Received* 15*th July*, 1996